THE ASTROPHYSICAL JOURNAL, 605:L69–L72, 2004 April 10

PARTICLE ACCELERATION IN MULTIPLE DISSIPATION REGIONS

KASPAR ARZNER[1] AND LOUKAS VLAHOS[2]
Received 2004 January 16; accepted 2004 February 24; published 2004 March 17

ABSTRACT

The sharp magnetic discontinuities that naturally appear in solar magnetic flux tubes driven by turbulent photospheric motions are associated with intense currents. Parker proposed that these currents can become unstable to a variety of microscopic processes, with the net result of dramatically enhanced resistivity and heating (nanoflares). The electric fields associated with such "hot spots" are also expected to enhance particle acceleration. We test this hypothesis by exact relativistic orbit simulations in strong random phase magnetohydrodynamic turbulence that is forming localized super-Dreicer Ohm electric fields ($10^2 \le E_\Omega/E_D \le 10^5$) occurring in 2%–15% of the volume. It is found that these fields indeed yield a large amplification of acceleration of electrons and ions and can effectively overcome the injection problem. We suggest in this article that nanoflare heating will be associated with sporadic particle acceleration.

Subject headings: acceleration of particles — turbulence

Understanding the mechanisms behind the dissipation of magnetic energy in the solar atmosphere is a key ingredient for the solution of several problems related to coronal heating, flares, and coronal mass ejections. Until recently, the study of magnetic energy dissipation seemed to follow two very distinctive paths: (1) phenomena related to the "quiet Sun" and coronal heating have been interpreted as continuous wave dissipation (Hollweg 1984; Ulmschneider, Rosner, & Priest 1991), and (2) flares, on the other hand, were associated with "impulsive" dissipation. Most flow charts proposed for the second process start with the formation of current sheets in comparably simple topologies (e.g., Priest & Forbes 2002), which reconnect, eject jets, and thereby drive turbulence. The turbulence, in turn, acts as a particle accelerator (Miller et al. 1997; Benz & Saint-Hilaire 2003) and finally dissipates into heat.

Parker (1983) questioned the split of magnetic dissipation in waves (for the heating) and current sheet formation (for the flare). He proposed instead that random photospheric footpoint motion forces the magnetic flux tubes to develop many tangential discontinuities throughout the corona and pointed out that the associated currents, when exceeding a critical value, will drive local instabilities that rapidly release the magnetic energy in what he called nanoflares. Macroscopically, the instabilities manifest as localized anomalous resistivity. The work of Parker was followed by many articles analyzing how the photospheric motions couple to the corona (Heyvaerts & Priest 1984; Cargill 1993; Gudiksen & Nordlund 2002). On a separate development, numerical studies of decaying resistive MHD turbulence reveal the formation of intense localized current sheets (Matthaeus & Lamkin 1986; Biskamp & Müller 2000), and simulations of nonlinear Alfvén waves in a single magnetic loop (Moriyashu et al. 2004) show the sporadic occurrence of slow and fast shocks–mode shocks as dissipative discontinuities. Parker's ideas and the numerical studies seem to share one important aspect: the intermittency of localized currents inside the large-scale structures.

Most of the literature triggered by Parker's well-known conjecture has focused on the role of nanoflares in coronal heating. The electric fields associated with the anomalous resistivity are, however, efficient particle accelerators as well. A simple yet realistic model for this kind of accelerator is homogeneous evolved MHD turbulence hosting intense localized current sheets. Models for particle acceleration using this scenario have been developed in the past (Matthaeus & Lamkin 1986; Ambrosiano et al. 1988), and a recent article studies the nonrelativistic test particle motion in the electromagnetic environment of fully developed isotropic turbulence (Dimitruk et al. 2003) with uniform resistivity.

Several observations seem to support the connection of heating with particle acceleration: the classical Lin et al. (1984) balloon observation of hard X-ray (HXR) microflares in active regions, ultraviolet (UV) subflares with HXR microflare counterparts (Porter et al. 1995), tiny flares at centimeter wavelengths that are associated with soft X-ray (SXR) transients (Gary et al. 1997), high-sensitivity observations of small decimetric reversed type III bursts (Benz et al. 2001) suggesting downward electron beams and high-located acceleration sites, acceleration without flares (Trottet 1994), SXR microevents with associated gyrosynchrotron radiation from the quiet Sun (Krucker et al. 1997), ubiquitous nanoevents from the quiet Sun observed in coronal extreme UV and radio radiation (Krucker & Benz 1998), and nonthermal tails in very small X-ray bursts (Krucker et al. 2002; Benz & Grigis 2002). In these observations, HXR and radio are believed to be a direct signature of nonthermal electrons, while SXR and (extreme) UV are secondary effects after thermalization.

In the present Letter we analyze the efficiency of particle acceleration in MHD turbulence with anomalous resistivity as a proxy for the solar corona. Unlike previous studies (Dimitruk et al. 2003; Gudiksen & Nordlund 2002), we assume that the resistivity is enhanced locally at the places where the "hot spots" appear.

Formation of hot spots.—We consider collisionless test particles in evolved homogeneous MHD turbulence with electromagnetic fields

$$\boldsymbol{B} = \boldsymbol{\nabla} \times \boldsymbol{A}, \tag{1}$$

$$\boldsymbol{E} = -\partial_t \boldsymbol{A} + \eta(\boldsymbol{j})\boldsymbol{j}, \tag{2}$$

where $\mu_0 \boldsymbol{j} = \boldsymbol{\nabla} \times \boldsymbol{B}$ and $\eta(\boldsymbol{j}) = \eta_0 \theta(|\boldsymbol{j}| - j_c)$ is an anomalous resistivity switched on above the critical current $j_c \sim \mathrm{enc}_s$ (Pa-

[1] Department of Particles and Matter, Laboratory for Astrophysics, Paul Scherrer Institut, 5232 Villigen PSI, CH-5232 Switzerland; arzner@astro.phys.ethz.ch.
[2] Department of Physics, Institute of Astronomy, Aristotle University, Thessaloniki 54124, Greece; vlahos@astro.auth.gr.

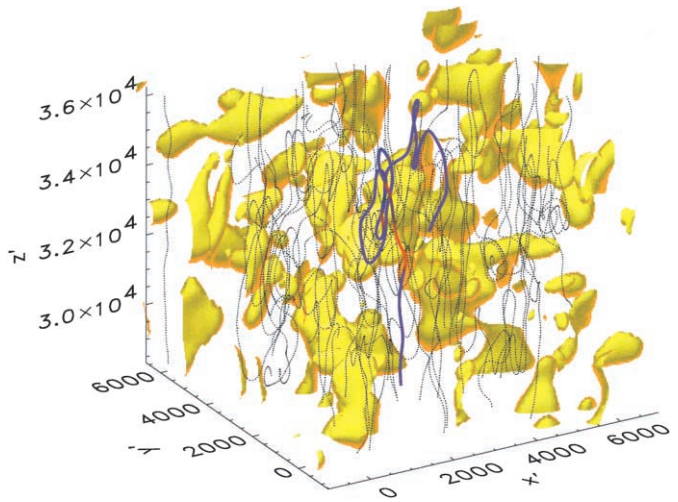

FIG. 1.—Localized dissipation regions $|\boldsymbol{j}| > j_c$ (*yellow*), magnetic field lines (*dotted*), and electron sample trajectory (*blue-red*, encodes $E_{\rm kin}$) for $l_x = l_y = 1$ km, $l_z = 20$ km, $\boldsymbol{B}_{\rm rms} = (2, 2, 10) \times 10^{-3}$ T, $B_0 = 2 \times 10^{-3}$ T, $E_\Omega/E_{\rm D} \sim 10^6$, and dissipative volume fraction 7%. The trajectory covers $2.6 \times 10^5 \Omega t$, and energetization occurs at dissipation regions.

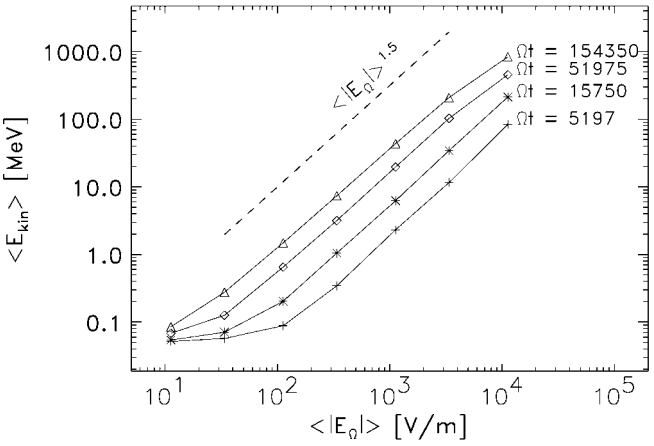

FIG. 3.—Dependence of the average proton energy at fixed time on the magnitude of the Ohmic field.

padopoulos 1977). Here $c_s(n)$ is the sound speed (number density) of the background plasma. The vector potential $\boldsymbol{A}(\boldsymbol{x}, t)$ is modeled as a random field, subject to the MHD constraints

$$\boldsymbol{E} \cdot \boldsymbol{B} = 0 \quad \text{if} \quad \eta(\boldsymbol{j}) = 0 \quad \text{and} \quad E/B \sim v_{\rm A}. \tag{3}$$

Equation (3) can be fulfilled in several ways. We use here a spectral form $\boldsymbol{A}(\boldsymbol{x}, t) = \sum_{\boldsymbol{k}} \boldsymbol{a}(\boldsymbol{k}) \cos[\boldsymbol{k} \cdot \boldsymbol{x} - \omega(\boldsymbol{k})\, t - \phi_k]$ in axial gauge, $\boldsymbol{a}(\boldsymbol{k}) \cdot \boldsymbol{v}_{\rm A} = 0$, and with dispersion relation $\omega(\boldsymbol{k}) = \boldsymbol{v}_{\rm A} \cdot \boldsymbol{k}$, which is an exact solution of the induction equation with a constant velocity field $\boldsymbol{v}_{\rm A}$. For simplicity, $\boldsymbol{A}(\boldsymbol{x}, t)$ is taken as Gaussian with random phases $\phi_{\boldsymbol{k}}$ and (independent) Gaussian amplitudes $\boldsymbol{a}(\boldsymbol{k})$ with zero mean and variance

$$\langle |\boldsymbol{a}(\boldsymbol{k})|^2 \rangle \propto (1 + \boldsymbol{k}^T S \boldsymbol{k})^{-\nu}. \tag{4}$$

A constant magnetic field B_0 along $\boldsymbol{v}_{\rm A}$ can be included without violating equation (3). The total MHD wave velocity is $v_{\rm A}^2 = \mathcal{B}^2(\mu_0 \rho)^{-1}$ with $\mathcal{B}^2 = B_0^2 + \sigma_B^2$ and $\sigma_B^2 = \frac{1}{2} \sum_{\boldsymbol{k}} |\boldsymbol{k} \times \boldsymbol{a}(\boldsymbol{k})|^2$ the magnetic fluctuations. The matrix $S = \mathrm{diag}(l_x^2, l_y^2, l_z^2)$ in equation (4) contains the outer turbulence scales, and the index ν determines the regularity of the two-point function at short distance. The presented simulations have $\nu = 1.5$, $\boldsymbol{v}_{\rm A} = (0, 0, v_{\rm A})$, and one turbulence scale is by an order of magnitude longer than the others, which describes migrating and reconnecting twisted flux tubes (see Fig. 1 for an illustration).

The vector potential contains some hundred wavevectors in the inertial shell $\min(l_i^{-1}) < |\boldsymbol{k}| < 10^{-2} r_{\rm L}^{-1}$, with $r_{\rm L}$ the rms thermal ion Larmor radius. We focus on strong turbulence ($\sigma_B/B_0 > 1$). The rms magnetic field $\mathcal{B}$ is a free parameter, which defines the scales of the particle orbits. The localized enhancement of the resistivity will (1) enhance the local heating inside the unstable current layer, $Q = \eta j^2$, forming what we call here hot spots. The fast heat transport away from the hot plasma will soon transform them to hot loops and will (2) dramatically enhance the particle (ion and electron) acceleration. The role of hot spots on coronal heating, their filling factor, and their statistical characteristics will be analyzed in a separate publication. We focus in this Letter on the role of hot spots as particle accelerators.

The physical units used in this study are selected to represent the solar atmosphere. In SI units and for typical values $\mathcal{B} \sim 10^{-2}$ T, $n \sim 10^{16}$ m^{-3}, and $T \sim 10^6$ K, the reference scales are as follows (electron values in brackets): time $\Omega^{-1} \sim 10^{-6}$ s (6×10^{-10} s); length $c\Omega^{-1} \sim 300$ m (0.17 m); thermal velocity $\sim 1.2 \times 10^5$ m s^{-1} (5×10^6 m s^{-1}); sound speed $c_s \sim 1 \times 10^5$ m s^{-1}; Alfvén speed $v_{\rm A} \sim 2 \times 10^6$ m s^{-1}; electron-ion col-

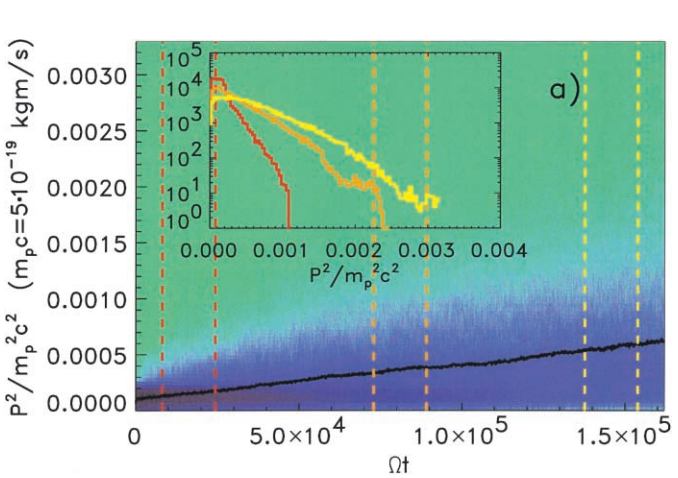

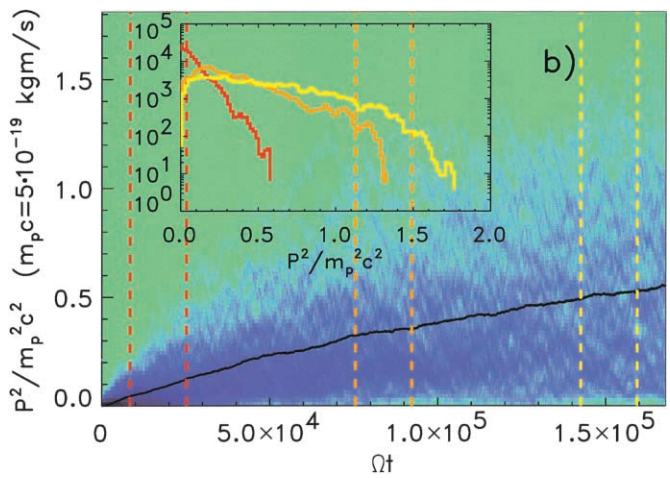

FIG. 2.—Evolution of proton kinetic momentum for $\mathcal{B} = 10^{-2}$ T, $B_0 = 10^{-3}$ T, and (*a*) $E_\Omega/E_{\rm D} \sim 10^3$ or (*b*) $E_\Omega/E_{\rm D} \sim 10^5$. *Solid line*: $\langle P'^2 \rangle$. *Insets*: P'^2-distribution in the dashed intervals. The initial population is maxwellian ($T = 10^6$ K).

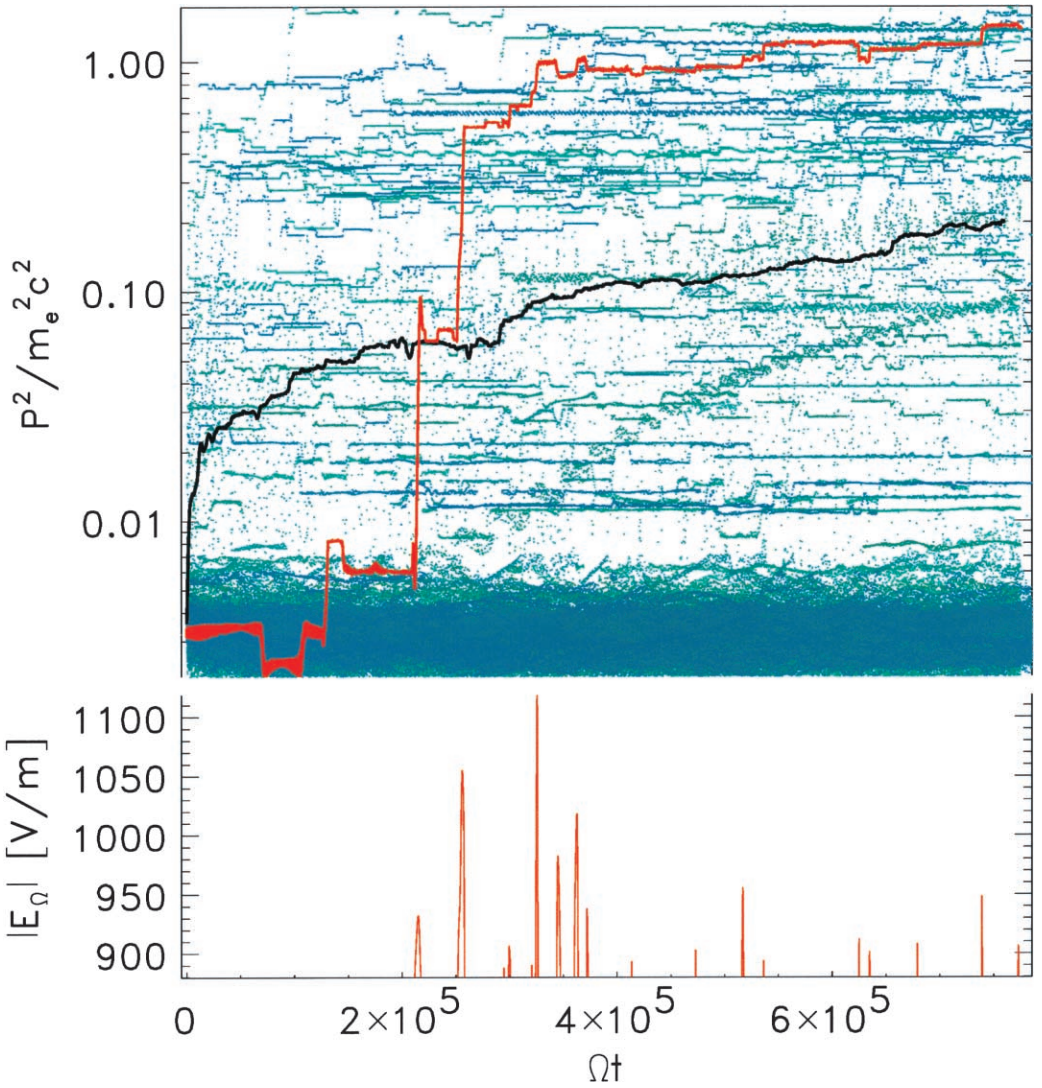

FIG. 4.—Evolution of electron kinetic momentum for $l_x = l_y = 1$ km and $l_z = 10$ km. Initial velocities are from the tail $v \geq 3\ v_{\rm th}$ of a maxwellian of 10^6 K. *Top*: Full population (*blue*), sample trajectory (*red*), and ensemble average (*black*). *Bottom*: Ohm field along the sample trajectory.

lision time $\tau \sim 0.003$ s; and Dreicer field $E_{\rm D} = ne^3 \ln \Lambda/(4\pi\epsilon_0^2 kT_e) \sim 3 \times 10^{-2}$ V m^{-1}. Time is measured in units of $\Omega^{-1} = m/q\mathcal{B}$; velocity in units of the speed of light; distance in units of $c\Omega^{-1}$.

Particle dynamics.—Particle momentum is measured in units of mc, vector potential in units of mc/q, magnetic field in units of $\mathcal{B}$, and electric current density in units of $\Omega\mathcal{B}/(\mu_0 c)$, so that the dimensionless threshold current is $j_c' = (m/m_p)c_s c/v_{\rm A}^2$. The electric field is measured in units of $c\mathcal{B}$, so that the dimensionless Dreicer field is $(v_e'/\tau')(m_e/m)$ with v_e' the electron thermal velocity and τ' the electron-ion collision time. The dimensionless (primed) equations of motion are

$$\frac{d\boldsymbol{x}'}{dt'} = \boldsymbol{v}', \tag{5}$$

$$\frac{d(\gamma \boldsymbol{v}')}{dt'} = \boldsymbol{v}' \times \boldsymbol{B}' - \frac{\partial \boldsymbol{A}'}{\partial t'} + \eta'(|\boldsymbol{j}'|)\boldsymbol{j}', \tag{6}$$

with γ the Lorentz factor, $\boldsymbol{B}' = \boldsymbol{\nabla}' \times \boldsymbol{A}'$, and $\boldsymbol{j}' = \boldsymbol{\nabla}' \times \boldsymbol{B}'$. The dimensionless resistivity η' is characterized by the resulting Ohm field $E_\Omega = \eta_0 |\boldsymbol{j}|$ relative to the Dreicer field $E_{\rm D}$. Equations (5) and (6) are integrated numerically.

When an initially maxwellian population is injected into the turbulent electromagnetic fields (eqs. [1]–[2]), the particles can become stochastically accelerated. Figure 2*a* shows the energy evolution of protons with initial temperature $T = 10^6$ K for the case $\eta' = 1.6 \times 10^{-6}$, corresponding to $E_\Omega/E_{\rm D} \sim 10^3$, which occurs in about 10% of the volume. The outer turbulence scales are $l_x' = l_y' = 3$ and $l_z' = 60$, and the rms magnetic field

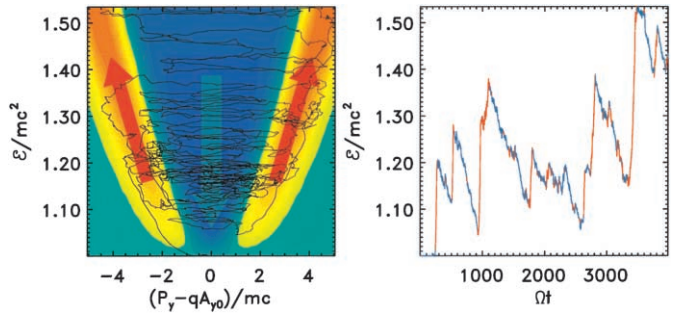

FIG. 5.—*Left*: Acceleration and deceleration domains in $(\mathcal{E}', P_y')$-space. Color code represents a theoretical estimate of the ensemble-averaged energy drift $d\langle\mathcal{E}'\rangle_\Omega/dt$. *Right*: Simulated energy evolution. Red (blue) color indicates positive (negative) theoretical $d\langle\mathcal{E}'\rangle_\Omega/dt$.

is $\mathcal{B} = 0.01T$, with a background contribution $B_0 = 0.001$ T along z. The density and temperature of the background plasma is 10^{16} m^{-3} and $T = 10^6$ K, so that $c_s' = 0.0004$ and $v_A' = 0.007$. For $\eta' = 0$ and since $\omega \ll \Omega$, the particle motion is approximately adiabatic (injection problem). Finite resistivity $\eta' > 0$ breaks adiabaticity, and energy can grow. The equation of motion (6) adds up—potentially—independent increments of kinetic momentum $\boldsymbol{P}' = \gamma \boldsymbol{v}'$, so that this quantity may be expected to behave diffusive. In fact, after a short initial phase, $\langle P'^2 \rangle$ increases linearly with time (Fig. 2*a*, $\langle P'^2 \rangle \sim t$). The momentum diffusion coefficient D (defined by $\langle P'^2 \rangle = A + Dt^{\alpha}$) increases, however, slower with η' than Var $(E_\Omega) \propto \eta'^2$, and above $E_\Omega/E_D \sim 5 \times 10^3$ subdiffusive behavior ($\alpha < 1$) is observed (Fig. 2*b*, $\langle P'^2 \rangle \sim t^{0.87}$). The average energy at fixed time increases then like $\eta'^{1.5}$ (Fig. 3). Acceleration is dramatically increased for ions, which can reach units of GeV in less than 60 ms. Standard diffusion ($\alpha \to 1$) is reached in the limit $\eta' \to 0$.

Because of their large inertia, protons gain energy in relatively small portions. This is not so for electrons. The momentum evolution of collisionless electrons of the high-energy tail of a maxwellian is shown in Figure 4. The plasma parameters are similar as in the proton case, but the maximum wavevector is somewhat smaller so that the volume fraction with $|\boldsymbol{j}| > j_c$ is 0.07 only. Since electrons have a much smaller Larmor radius, they follow the field lines perfectly adiabatically and gain energy only when dissipation regions are encountered (Fig. 1). The orbits then exhibit large energy jumps (Fig. 4), so that a Fokker-Planck description is inappropriate.

In order to gain physical insight into the interplay of electric acceleration and magnetic confinement, we consider the space of the two approximate invariants of our model, energy $\mathcal{E}$ and canonical momentum along the adiabatic direction, as illustrated in Figure 5 (*left*). Here, y is the slowly varying direction, and the background magnetic field is represented by $A_{y0} = B_0 x$. Color code represents a theoretical estimate on $d\langle \mathcal{E}' \rangle_\Omega/dt = \langle \eta' \boldsymbol{j}' \cdot \boldsymbol{v}' \rangle$, obtained by assuming constant particle density on surfaces of constant $\mathcal{E}$ and P_y. The tremulous line in Figure 5 (*left*) is a sample trajectory, whose energy evolution is shown in Figure 5 (*right*). Red (blue) color indicates positive (negative) theoretical $d\langle \mathcal{E}' \rangle_\Omega/dt$. As can be seen, the theoretical (ensemble) estimate is statistically sharp enough to reflect in an individual trajectory. The underlying mechanism is purely geometrical: conservation of P_y' and $\mathcal{E}'$ restricts A_y' to a band $(A_y' - P_y')^2 \le \mathcal{E}'^2 - 1$, and since A_y is positively correlated to $E_y \sim -\Delta A_y$, the instantaneous value of $d\mathcal{E}_\Omega'/dt' \sim E_y' v_y'$ can be guessed from P_y' and $\mathcal{E}'$ (Arzner et al. 2002). As a result, particles drift toward higher energy in the red domain of Figure 5 (*left*) until they are scattered into the blue domain, where they sink to the boundary of the red domain. In spatially homogeneous turbulence this life cycle repeats indefinitely.

Summary.—We have investigated the effect of resistive hot spots on coronal stochastic acceleration, with evolved MHD "turbulence" modeled by Gaussian fields. The hot spots form sporadically when the electric current exceeds a critical threshold. They do not only create localized Ohmic heating (as a possible coronal heating mechanism) but are also efficient particle accelerators:

1. For vanishing resistivity, the ions are slowly accelerated (second-order Fermi) and the electrons remain adiabatic. As resistivity increases at the hot spots, ions and electrons are accelerated efficiently.
2. Acceleration is not sensitive to the type of low-frequency MHD waves used as long as these are able to form tangential discontinuities and drive locally unstable currents that will enhance the resistivity.
3. The acceleration mechanism proposed overcomes the injection problem.
4. Heating and acceleration may have a common origin.
5. Numerous well-known observations can possibly be explained, i.e., long-lasting acceleration, type III bursts before the flare or without flares, nonthermal X-ray emission from microflares, and nonthermal emission from the quiet Sun.

Several important aspects are still missing from our current analysis. The first is the non-Gaussian nature of real MHD turbulence, with formation of larger scale intermittent structures. Second, the local reconstruction of magnetic fields (Parker 1993) will drive nonlinearly stable discontinuities and create avalanches, as was proposed by Lu & Hamilton (1991) and Vlahos et al. (1995). Finally, the neglection of collisions of energetic particles breaks down on timescales of seconds in the solar corona.

We suggest that the hot spots developed naturally inside a turbulent plasma can be any type of flare, i.e., nanoflare, microflare, or a regular flare, depending on the sharpness of the discontinuity and the value of the resistivity associated with the unstable current. On the basis of the above analysis, we believe that reconnection is hosted by turbulence and not the opposite. Although we have envisaged parameters representing the solar corona, the mechanism may have applications to other astrophysical situations such as turbulent jets, upstream of shocks, or turbulence in accretion disks.

We thank A. Benz for helpful discussions. This work has received partial support from the European Research Training Network under contract NPRN-eT-2001-00310.

REFERENCES

Ambrosiano, J., Mattheus, W. H., Goldstein, M. L., & Plante, D. 1988, J. Geophys. Res., 93, 14383
Arzner, K., Scholer, M., & Treumann, R. A. 2002, J. Geophys. Res., 107, 10029
Benz, A. O., & Grigis, P. 2002, Sol. Phys., 210, 431
Benz, A. O., Messmer, P., & Monstein, C. 2001, A&A, 366, 326
Benz, A. O., & Saint-Hilaire, P. 2003, Adv. Space Res., 32, 2415
Biskamp, D., & Müller, W. C. 2000, Phys. Plasmas, 7, 4889
Cargill, P. 1993, Sol. Phys., 147, 263
Dimitruk, P., Mattheus, W. H., Seenu, N., & Brown, M. R. 2003, ApJ, 597, L81
Gary, D. E., Hartl, M., & Shimizu, T. 1997, ApJ, 477, 958
Gudiksen, B. V., & Nordlund, Å. 2002, ApJ, 572, L113
Heyvaerts, J., & Priest, E. R. 1984, A&A, 137, 63
Hollweg, J. V. 1984, ApJ, 277, 392
Krucker, S., & Benz, A. O. 1998, ApJ, 501, L213
Krucker, S., Benz, A. O., Bastian, T. S., & Acton, L. W. 1997, ApJ, 488, 499
Krucker, S. Christe, S., Lin, R. P., Hurford, G. J., & Schwartz, R. A. 2002, Sol. Phys., 210, 445
Lin, R. P., Schwartz, R. A., Kane, S. R., Pelling, R. M., & Hurley, K. C. 1984, ApJ, 283, 421
Lu, E. T., & Hamilton, R. J. 1991, ApJ, 380, L89
Matthaeus, W. H., & Lamkin, S. L. 1986, Phys. Fluids, 29, 2513
Miller, J. A., et al. 1997, J. Geophys. Res., 102, 14631
Moriyashu, S., Kudoh, T., Yokoyama, T., & Shibata, K. 2004, ApJ, 601, L107
Papadopoulos, K. 1977, Rev. Geophys. Space Phys., 15, 113
Parker, E. N. 1983, ApJ, 264, 635
———. 1993, ApJ, 414, 389
Porter, J. G., Fontenla, J. M., & Simnett, G. M. 1995, ApJ, 438, 472
Priest, E. R., & Forbes, T. G. 2002, A&A Rev., 10, 313
Trottet, G. 1994, Space Sci. Rev., 68, 140
Ulmschneider, P., Priest, E. R., & Rosner, R., eds. 1991, Mechanisms of Chromosphere and Coronal Heating (Berlin: Springer)
Vlahos, L., Georgoulis, M., Kluiving, R., & Paschos, P. 1995, A&A, 299, 897